Hierarchical Pattern Replication by Polymer Demixing**

By *Monika Sprenger*, *Stefan Walheim*, *Claudia Schäfle*, and *Ullrich Steiner**

The replication of patterns on sub-micrometer lateral length scales is of considerable technological interest.[1] While photolithography is firmly established for the replication of patterns on micrometer and sub-micrometer length scales, there is an increasing interest in alternative technologies. This is partly due to the fact that photolithography is facing an intrinsic limitation, given by the wavelength of light. A second, equally important motivation is the search for simple, low-cost techniques for the reliable replication of micrometer sized patterns. Such a technology could be an integral part in the future manufacture of all-polymer semiconducting devices, such as integrated circuits or display elements.

The emergence of microcontact printing a decade ago[2] inspired the development of a large number of different soft-lithography techniques.[3] Alternative methods include nanoimprinting,[4,5] embossing, and injection molding.[6] Typically, these techniques work best at a lateral resolution of 1 μm and larger, but structures sizes down to 10 nm have also been reported.[3] More recently, film instabilities were employed to replicate lateral patterns.[7–9] These methods harness characteristic modes that develop during a spontaneous (spinodal) film instability caused by electric fields[9] or temperature gradients.[10] In addition to surface instabilities, phase morphologies of a binary polymer blend that form during the demixing have also been used as a lithographic technique.[7,11]

Most of the pattern replication methods listed above share, however, two limitations: i) the lateral structure size is given by (and therefore limited to) the resolution of the master, and ii) they are limited to the replication of structures with relatively small aspect ratios (height/width of individual features). While pattern replication on a 100 nm scale was reported in some cases, the extension of most soft-lithography techniques to lateral structure sizes significantly below 1 μm is often cumbersome and unreliable.

Here, we demonstrate a new technique that allows one to create structures with a lateral size of ≈ 100 nm, which are registered with respect to a substrate pattern. Our method makes use of the rich phase morphology that develops during the demixing of a three-component polymer mixture.[12] Since in a thin film polymer demixing is strongly modified by the film surfaces, all three polymer components can be aligned with respect to a surface energy pattern that was created by microcontact printing.[7] The advantage of using a ternary (rather than a binary) blend is the ability to generate structure sizes that are significantly smaller than the lateral dimension imposed by the surface energy pattern.

The ternary polymer mixture used in this study consisted of polystyrene (PS) with molecular weight $M_w = 94.9$ kg/mol and polydispersity index $M_w/M_n = 1.06$; poly(methyl methacrylate) (PMMA) with $M_w = 126$ kg/mol, $M_w/M_n = 1.04$; and poly(2-vinylpyridine) (PVP) with $M_w = 115$ kg/mol, $M_w/M_n = 1.03$. The polymers were dissolved in analytic grade cyclohexanone. Typical solution concentrations were 3 % polymer by weight. The substrates used were highly polished silicon wafers (donated by Wacker Chemie GmbH). The wafers were cleaned in a jet of carbon dioxide crystals ("snowjet").[13] The substrates were then first covered with a ≈ 2 nm thick titanium layer, followed by a 20–30 nm thick gold layer. The surfaces were further modified by depositing a complete or patterned self-assembled alkane monolayer (SAM) onto the gold covered substrate. To obtain laterally homogeneous SAM layers, the substrates were immersed overnight in a 0.285 % solution of octadecylmercaptan in an 5:2 ethanol/THF mixture.

Patterned SAM layers on Au were made by microcontact printing (μCP),[3] using a colloidal stamp.[14,15] Colloidal stamps make use of a hexagonally close-packed monolayer of colloidal spheres that forms, when a drop of a colloidal suspension dries under suitable conditions.[16] A rubber stamp was made by pouring polydimethysiloxane (PDMS) onto the colloidal layer, which is subsequently crosslinked to form a rubber (Sylgard 184, Dow Corning). After releasing the rubber from the colloid covered surface, the stamp has assumed the pattern of the colloidal layer (Fig. 1a). Depending on the

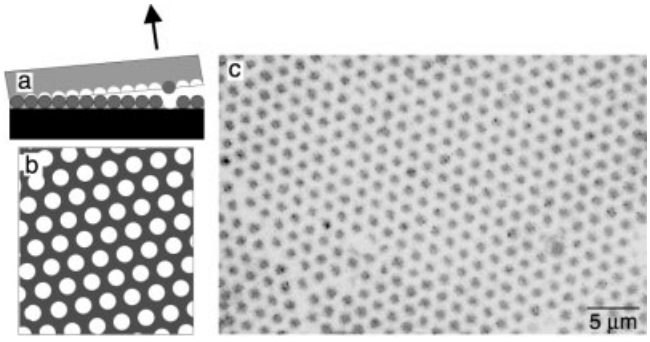

Fig. 1. Microcontact printing using a colloidal stamp. a) Schematic representation of the stamp preparation. PDMS is poured onto a self-assembled colloidal monolayer and crosslinked. During the release of the stamp, most colloidal spheres remain on the substrate, leading to the stamp surface schematically shown in (b): hemispherical holes (white) in the rubber matrix (gray). c) Visualization of a Au surface after μCP of an alkane-thiol SAM using a stamp made from colloidal spheres with a diameter of 1.7 μm. To obtain the contrast in the optical image, the Au was etched away from the surface areas not protected by the stamped SAM.

[*] Prof. U. Steiner
Department of Polymer Chemistry and Materials Science Center
University of Groningen
NL-9747 AG Groningen (The Netherlands)
E-mail: u.steiner@chem.rug.nl
M. Sprenger,[+] Dr. S. Walheim,[++] C. Schäfle
Fachbereich Physik, Universität Konstanz
D-78457 Konstanz (Germany)
[+] Present address: Max-Plank Institut für Metallforschung, D-70569 Stuttgart, Germany.
[++] Present address: Institut für Nanotechnologie, Forschungszentrum Karlsruhe, D-76021 Karlsruhe, Germany.

[**] We thank W. Zulehner and Wacker-Chemie GmbH for supplying the silicon wafers. This work was partially funded by the Deutsche Forschungsgemeinschaft (DFG) through the Sonderforschungsbereich 513 and the priority program of the DFG "wetting and structure formation at surfaces", and by the Dutch "Stichting voor Fundamenteel Onderzoek der Materie" (FOM).

 DOI: 10.1002/adma.200304463

ADVANCED MATERIALS

details of the processing conditions, the colloidal spheres are either embedded in the rubber stamp or they stay behind on the surface, giving rise to a negative replica of the colloidal surface (Fig. 1b). We used a colloidal stamp with the negative replica of a hexagonally packed layer of colloids with a diameter of 1.7 μm. The structured surface of the stamp was soaked in an octadecylthiol solution (1 mmol in ethanol) and the stamp was placed onto a Au surface. This causes the formation of a SAM in the places where the rubber stamp touches the Au surface.

The result of this μCP procedure is visualized in Figure 1c. To reveal the patterned SAM, the substrate was exposed for several minutes to a cyanide solution (1 mol potassium thiosulfate, 0.1 mol potassium ferricyanide, 0.01 mol potassium hexacyanoferrate(II) trihydrate, 10 mol potassium hydroxide in H_2O), which etches away the Au at the locations that are not protected by a SAM layer. The optical micrograph in Figure 1c mirrors the symmetry of the colloidal monolayer: a hexagonal pattern of circular polar surface areas in a non-polar matrix formed by the SAM. The optical contrast in Figure 1c stems from the variation in the optical reflectivity (Au vs. silicon), which was caused by the etching step.

Polymer films were prepared by spin-coating from PS/PMMA/PVP solutions (typically at 3000 rotations per minute) onto both types of surfaces (homogeneous and patterned SAM layers). The average film thickness was approximately 100 nm. After spin-coating, the films were analyzed by contact mode atomic force microscopy (AFM).

We start by discussing the phase morphology of films deposited onto homogeneous SAM surfaces. In Figure 2a, a characteristic phase morphology of a PS/PMMA/PVP blend after spin-coating from cyclohexanone is shown. On the non-polar SAM surface, all three phases form a lateral pattern that spans from the substrate to the air surface of the film in a quasi-two-dimensional lateral arrangement. The type of pattern

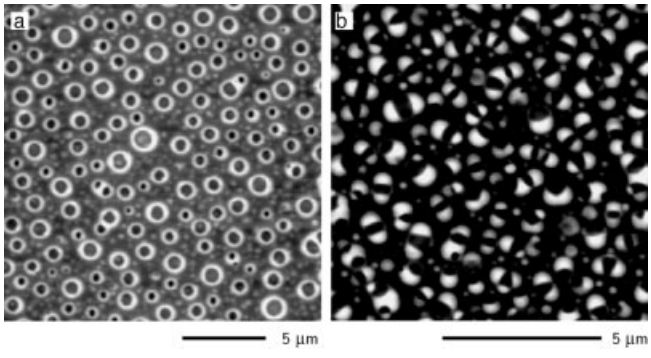

Fig. 2. Demixing of a PS/PMMA/PVP (3:1:1) blend on a SAM covered Au surface during spin-coating from cyclohexanone in a dry atmosphere. The AFM image in (a) shows circular inclusions of PVP embedded in a PS matrix. The bright rings are the PMMA phase that is intercalated at the PS/PVP interface. The PS and PVP phases can be removed by sequentially washing the sample in ethanol and cyclohexane. This leads to isolated PMMA rings on the surface [17]. The sample in (a), spin-cast at a high ambient humidity (≈60 %), exhibits the complete wetting of PMMA of the PS/PVP interface, while the similarly prepared sample shown in (b), which was spin-cast in a nitrogen flow (humidity < 20 %) showed partial wetting of PMMA (bright) of the PS/PVP interface. The gray scale contrast corresponding to the height variation is ≈ 50 nm.

that is formed depends on the relative ratios of the three components in the blend.[12] We focus here on a PS/PMMA/PVP mixing ratio of 3:1:1. This results in a PS matrix phase, in which the PMMA and PVP phases are embedded.

The lateral arrangement of the three phases is determined by the balance of their mutual interfacial tensions γ (which are related to the Flory–Huggins enthalpic interaction parameters). Two regimes can be distinguished.[17] If $\gamma_{PS/PMMA} + \gamma_{PMMA/PVP} < \gamma_{PS/PVP}$, the overall interfacial energy in the blend is lowered by intercalating PMMA at all PS/PVP interfaces. This corresponds to the complete wetting of the PS/PVP interface by PMMA as shown in Figure 2a. If, on the other hand $\gamma_{PS/PMMA} + \gamma_{PMMA/PVP} > \gamma_{PS/PVP}$, the PS/PVP interface is only partially wetted by PMMA, leading to PMMA and PVP domains that lie side-by-side in the PS matrix (Fig. 2b). The films in Figures 2a,b were made from the same solution on identically prepared substrates, but they were spin-cast at differing ambient humidities.[17] We attribute the differing phase morphologies to the water uptake of the hygroscopic PVP phase when spin-coating at varying ambient humidities, facilitated by the condensation of water onto the film. At high humidities (≈60 %, Fig. 2a), this effect is expected to be more significant compared to a spin-coating experiment at lower humidities (< 20 %, Fig. 2b). A difference in water uptake results in a strong variation of $\gamma_{PS/PVP}$, causing a cross-over between partial and complete interfacial wetting of the PMMA phase.[17]

For our experiments, it is essential to obtain the morphology shown in Figure 2a. This can either be achieved by spin-coating from cyclohexanone at a high enough humidity or by spin-coating PS/PMMA/PVP mixtures from THF, which yields the morphology of Figure 2a, irrespective of the humidity. We chose to work from cyclohexanone at a high humidity, since the spin-coating of thin polymer films from THF often results in films with long wavelength surface undulations.[17]

Before proceeding, it is useful to summarize the main features of Figure 2a:

- The PMMA phase forms a continuous layer at the PS/PVP interface that extends from the substrate to the air surface.
- The width of the PMMA rings is independent of the characteristic lateral length scale (i.e., the mean distance between the PVP phases) that forms during demixing. It is determined by relative amount of PMMA in the blend.
- It is possible to remove the PS and PVP phases, leaving behind essentially unaltered PMMA rings.[12,17]

These three observations allow us to make use of the PMMA phase morphology in a lithographic process. To this end, the polymer solution that was used in Figure 2 was cast onto a Au surface that had a hexagonally prepatterned SAM layer. Figures 3a,b reveal a phase morphology that mirrors the underlying SAM pattern: i) instead of the polydisperse distribution of ring sizes in Figure 2a, the rings in Figures 3a,b are all of the same size, and ii) the rings are aligned on a hexagonal grid reflecting the SAM pattern that was printed by the colloidal stamp.

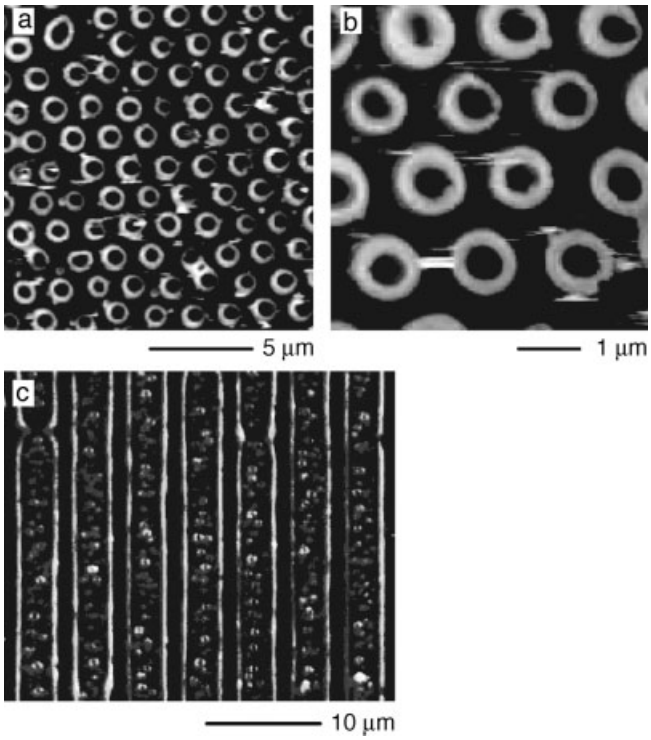

Fig. 3. Demixing of the PS/PMMA/PVP solution from Figure 2 on a Au substrate that was prepatterned using a colloidal stamp. After spin-coating, the phase morphology from Figure 2a has aligned with respect to the substrate surface energy pattern. The more polar PVP has segregated onto the bare Au domains, displacing the PS to the non-polar substrate regions. The PMMA phase (shown in the AFM images in (a,b) after the removal of PS and PVP) wets the PS/PVP interface, thereby mirroring the hexagonal pattern of the colloidal stamp. The reduced image quality in (a) is due to the low adhesion of the PMMA rings to the substrate, rendering AFM imaging somewhat more difficult. In (c), a 2:1:2 PS/PMMA/PVP mixture was spin-cast from THF onto a stripe-patterned substrate. The PMMA has segregated to the edges of the 3 μm wide SAM covered stripes, leading to the formation of PMMA stripes, whose width (~300 nm) is a factor of 10 smaller than the template structure width. In addition, the optical image shows PMMA and PVP inclusions in the PS stripes. The imperfect replication of the striped surface energy pattern of the substrate is presumably due to a non-optimal composition of the PS/PMMA/PVP blend. The gray scale contrast corresponding to the height variation is ≈ 120 nm.

The origin of the ordering process that lead to the phase morphology in Figure 3 is analogous to the case of a binary mixture.[7] The more polar PVP phase segregates preferentially onto the more polar Au surface (black regions in Fig. 1c), displacing the less polar PS phase onto the non-polar SAM surface regions (bright in Fig. 1c). This leads to a hexagonal arrangement of cylindrical PVP inclusions with a spacing of the cylinder centers of 1.7 μm, given by the diameter of the colloids. Since PMMA wets the PS/PVP interfaces, it forms a mantle around the PVP columns. After dissolving the PS and PVP phases, the lateral arrangement of rings mirrors the arrangement of the PVP columns.

The ring pattern in Figures 3a,b displays three distinct length scales. The inter-ring spacing is given by the hexagonal substrate grid, determined by the size of the colloidal spheres. Second, the diameter of the rings is determined by PS/PVP composition ratio, and third, the wall thickness of the rings reflects the relative amount of PMMA in the blend. The three length scales are essentially independent of each other. It should therefore be possible to vary them within certain limits. In particular, the PMMA wall width of 200–300 nm is one order of magnitude smaller than the lattice spacing of 1.7 μm and is comparable to the height of the rings of ≈ 100 nm (given by the thickness of the film after spin-coating).

Finally, we discuss the limitation of our pattern replication technique. In Figure 3c, a 2:1:2 PS/PMMA/PVP mixture was spin-cast from THF onto a Au surface, which had a striped SAM pattern. The principle discussed above—the segregation of PMMA at the PS/PVP interface—is also discernible here. PMMA has segregated to the interface between the PS and PVP phases, which have segregated to the SAM covered and bare Au regions of the substrate, respectively. Also here, the PMMA stripe width of ~300 nm is smaller by a factor of 10 compared to the SAM stripe width of 3 μm. We observe in addition small circular inclusions of PVP and PMMA in the PS phase. They are presumably due the choice of the PS/PMMA/PVP mixing ratio. Apparently, not all the PVP was accommodated on the Au stripes, leading to the spurious PVP inclusions, decorated by the PMMA rings. This illustrates the need to carefully select the mixing ratio of the two majority phases to achieve good replication results, thereby limiting the choice of the second length scale discussed above.

It is interesting to compare the lateral control of demixing of binary and ternary polymer blends. Fukunaga et al.[18] have investigated the demixing of a binary polymer blend on a substrate with a sub-100 nm pattern. While the surface pattern influences the demixing process, the polymer domains are not in register with the underlying surface pattern. In contrast, by using a ternary polymer blend, it is possible to make use of the competition of interfacial energies (i.e., a competition between the intercalation of PMMA at the polymer/polymer interface versus the polymer/substrate interface) to achieve a control of phase morphologies on a 100 nm length scale.

In summary, we have demonstrated a new replication method that is based on the demixing of a ternary polymer mixture during spin-coating. The technique relies on the interfacial wetting of one of the polymer components at the interface of the other two. The two majority phases align with respect to a pattern in the substrate surface energy (created by microcontact printing), thereby resulting in a lithographically reproduced structure of the interfacially active minority phase. In particular, the structure width achieved this way is significantly smaller than the lateral dimensions of the substrate prepattern. Our technique should be expandable to other polymer mixtures. The main requirement for the choice of materials is the interfacial wetting of one component at the interface of the other two.

Received: September 26, 2002
Final version: January 17, 2003

[1] K. Ziemelis, *Nature* **2000**, *406*, 1021.
[2] A. Kumar, G. M. Whitesides, *Appl. Phys. Lett.* **1993**, *63*, 255.
[3] Y. Xia, G. M. Whitesides, *Angew. Chem.* **1998**, *110*, 568.
[4] S. Y. Chou, P. R. Krauss, *Science* **1996**, *272*, 85.
[5] S. Y. Chou, C. Keimel, J. Gu, *Nature* **2002**, *417*, 835.
[6] H. Schift, C. David, M. Gabriel, J. Gobrecht, L. Heyderman, W. Kaiser, S. Köppel, L. Scandella, *Microelectron. Eng.* **2000**, *53*, 171.

ADVANCED MATERIALS

[7] M. Böltau, S. Walheim, J. Mlynek, G. Krausch, U. Steiner, *Nature* **1998**, *391*, 877.
[8] S. Y. Chou, L. Zhuang, L. Guo, *Appl. Phys. Lett.* **1999**, *75*, 1004.
[9] E. Schäffer, T. Thurn-Albrecht, T. P. Russell, U. Steiner, *Nature* **2000**, *403*, 874.
[10] E. Schäffer, S. Harkema, R. Blossey, U. Steiner, *Europhys. Lett.* **2002**, *60*, 255.
[11] A. Karim, J. F. Douglas, B. P. Lee, J. A. Rogers, R. J. Jackman, E. J. Amis, G. M. Whitesides, *Phys. Rev. E* **1998**, *57*, 273.
[12] S. Walheim, M. Ramstein, U. Steiner, *Langmuir* **1999**, *15*, 4828.
[13] R. Sherman, D. Hirt, R. J. Vane, *J. Vac. Sci. Technol.* **1994**, *12*, 1876.
[14] Y. Xia, J. Tien, D. Qin, G. Whitesides, *Langmuir* **1996**, *12*, 4033.
[15] C. Bechinger, H. Muffler, C. Schäfle, O. Sundberg, P. Leiderer, *Thin Solid Films* **2000**, *366*, 135.
[16] F. Burmeister, C. Schäfle, B. Keilhofer, C. Bechinger, J. Boneberg, P. Leiderer, *Adv. Mater.* **1998**, *10*, 495.
[17] M. Sprenger, S. Walheim, A. Budkowski, U. Steiner, *Interface Sci.* **2003**, *11*, 225.
[18] K. Fukunaga, H. Elbs, G. Krausch, *Langmuir* **2000**, *16*, 3474.

Palladium Nanotubes with Tailored Wall Morphologies

By *Martin Steinhart*, *Zhihong Jia*, *Andreas K. Schaper*, *Ralf B. Wehrspohn*,* *Ulrich Gösele*, and *Joachim H. Wendorff*

Nanotubes have an outstanding potential to transport or store gases and fluids for fuel cells, energy conversion, catalysis, and drug release.[1–10] Nanotube walls with an internal fine structure and thus a high specific interface area should strongly enhance the reactivity as well as the capability for adsorption. Furthermore, the efficiency of transport processes within and across the nanotube walls should be improved. We report on a simple method to generate nanotubes with controllable wall morphology or porosity in the nanometer range. It consists of three steps: the formation of multi-component nanotubes; demixing to generate coexisting phases within the tube walls; and the controlled ripening of the phase morphology. Depending on the selected components, their concentrations, and the ripening stage, nanotubes with characteristic wall morphologies were obtained. Selective removal of one component yields residual nanotubes with a specific nanoroughness and a controllable porosity. This fundamental concept should be applicable to a broad range of materials. We will demonstrate this exemplarily by means of structured palladium nanotubes, since palladium nanoparticles are of considerable interest for catalysis,[11–14] sensor technology,[15] and hydrogen storage.[16]

Decomposition in thin films on smooth substrates has been investigated extensively.[17] Spinodal demixing induced either by a thermal quench or by the evaporation of a solvent generates a co-continuous phase morphology with a characteristic length. Simultaneously, ripening occurs to reduce the initially large internal interface area. The phase morphology is strongly affected by substrate/film and film/air interfaces, as well as by confinement effects.[18–22] Several groups have used thin films structured by phase separation for devices such as transistors,[23] light emitting diodes,[24] or photodiodes.[25] It would be advantageous if nanotubes with such well-defined morphologies could be obtained in a controlled way. However, to date, the range of wall morphologies accessible by preparation methods such as self-assembly[1–5] and the use of templates[6–10] is limited to core–shell structures via consecutive synthetic steps.[6,10] Our approach is based on wetting porous matrices that exhibit high surface energies with multicomponent melts or solutions containing polymers.[26] A mesoscopic film of the wetting liquid covers the pore walls rapidly, since polymers adsorb avidly on high energy surfaces.[27] A kinetically stable stationary state is generated when all adsorption sites on the pore wall are occupied. Solidification of the wetting liquid at this stage results in the preservation of nanotubes. Decomposition can be induced by solvent evaporation during wetting or by thermal quenching. Ripening occurs after the onset of phase separation, as long as the solvent concentration is sufficiently high to prevent solidification, or if the system is annealed at temperatures where at least one component is liquid. Freezing of the ripening process can be achieved by cooling below the glass temperature of a polymeric component, by the onset of crystallization, by crosslinking, or by the selective removal of one component. Wall morphologies ranging from a molecular-disperse distribution of the components to co-continuous networks or matrix-dispersed particles should be accessible.

To prepare palladium nanotubes, we wetted ordered, porous alumina[28] with solutions containing poly(D,L-lactide) (PDLLA) and palladium(II) acetate ($Pd(OAc)_2$) in a ratio of 1:1, under ambient conditions. Solid PDLLA/$Pd(OAc)_2$ nanotubes were obtained after the solvent (dichloromethane or chloroform) was evaporated. Phase separation took place when the solvent concentration fell below a certain threshold. Annealing at 200 °C led to the thermal degradation of $Pd(OAc)_2$ within a few tens of seconds and Pd^{II} was reduced to Pd^0. The formation of polycrystalline face-centered cubic (fcc) palladium was confirmed by selected-area electron diffraction (SAED). Figure 1a shows a transmission electron microscopy (TEM) image of an ultrathin section of porous alumina (pore diameter $D_p = 55$ nm, pore depth $t_p = 50$ μm) after wetting and annealing for 5 min at 200 °C. The pore walls are covered by a PDLLA/Pd layer with a thickness of about 10 nm that does not exhibit a pronounced internal morphology. Some palladium nanoparticles, a few nanometers in size,

[*] Prof. R. B. Wehrspohn, M. Steinhart, Prof. U. Gösele
Max-Planck-Institute of Microstructure Physics
Weinberg 2, D-06120 Halle (Germany)
email: wehrspoh@mpi-halle.de
M. Steinhart, Prof. J. H. Wendorff
Institute of Physical Chemistry, Philipps-Universtity
Hans-Meerwein Strasse, D-35032 Marburg (Germany)
Z. Jia, Dr. A. K. Schaper, Prof. J. H. Wendorff
Center of Material Science, Philipps-Universtity
Hans-Meerwein Strasse, D-35032 Marburg (Germany)

[**] Support from the Deutsche Forschungsgemeinschaft (WE 2637/1-1 and WE 496/19-1) and the donation of polylactides form Böhringer Ingelheim are gratefully acknowledged. We thank Petra Göring, Jinsub Choi, Kornelius Nielsch, Katrin Schwirn, Stefan Schweizer, Jörg Schilling, and Sven Matthias for the preparation of the templates, as well as Dr. H. Hofmeister for additional TEM investigations.

  DOI: 10.1002/adma.200304502